Available online at www.sciencedirect.com
ScienceDirect
Trans. Nonferrous Met. Soc. China 26(2016) 589−598
Transactions of Nonferrous Metals Society of China
www.tnmsc.cn

Electrochemical behavior of mesh and plate oxide coated anodes during zinc electrowinning

Wei ZHANG[1,2], Michael ROBICHAUD[2], Edward GHALI[2], Georges HOULACHI[3]

1. School of Metallurgical Engineering, Hunan University of Technology, Zhuzhou 412007, China;
2. Department of Mining, Metallurgy and Material Engineering, Laval University, Ste-Foy, Quebec G1K 7P4, Canada;
3. Hydro-Quebec Research Center, Shawinigan, Quebec G9N 7N5, Canada

Received 2 February 2015; accepted 31 October 2015

Abstract: The catalytic performance of two oxides coated anodes (OCSs) meshes and one OCA plate was investigated in a zinc electrowinning electrolyte at 38 °C. Their electrochemical behaviors were compared with that of a conventional Pb−0.7%Ag alloy anode. Electrochemical measurements such as cyclic voltammetric, galvanostatic, potentiodynamic, open-circuit potential (OCP) and in situ electrochemical noise measurements were considered. After 2 h of OCP test, the linear polarization shows that the corrosion current density of the Ti/(IrO_2−Ta_2O_5) mesh electrode is the lowest (3.37 μA/cm^2) among the three OCAs and shows excellent performance. Additionally, after 24 h of galvanostatic polarization at 50 mA/cm^2 and 38 °C, the Ti/MnO_2 mesh anode has the highest potential (1.799 V), followed by the Ti/(IrO_2−Ta_2O_5) plate (1.775 V) and Ti/(IrO_2−Ta_2O_5) mesh (1.705 V) anodes. After 24 h of galvanostatic polarization followed by 16 h of decay, the linear polarization method confirms the sequence obtained after 2 h of OCP test, and the Ti/(IrO_2−Ta_2O_5) mesh attains the lowest corrosion current density. The Ti/(IrO_2−Ta_2O_5) mesh anode also shows better performance after 24 h of galvanostatic polarization with the overpotential lower than that of the conventional Pb−Ag anode by about 245 mV.

Key words: oxides coated anode; mesh; plate; electrochemical measurement; electrochemical behavior

1 Introduction

In the zinc electrowinning industry, a considerable amount of energy is expended to overcome the high overpotential of the oxygen evolution reaction at the anode. Considering the industrial significance, it is necessary to reduce this overpotential. Most currently proposed systems utilize an oxides coated anode (OCA) based on a titanium substrate coated with a material that is catalytic toward oxygen evolution. The most common base used for OCAs is titanium [1]. Dimensionally stable anodes (DSAs) consist of mixed metal-oxide coatings, usually on titanium or nickel substrates [2]. The oxides that can be used in the oxide coatings include tantalum oxide (Ta_2O_5), iridium oxide (IrO_2), ruthenium oxide (RuO_2), tin oxide (SnO_2), etc. [3−6]. MSINDO et al [2] found that a DSA plate had a higher corrosion resistance than a DSA mesh. Additionally, for the DSA coated with iridium oxide, the surface electrochemistry for the DSA mesh and plate is controlled by the Ir(III)/Ir(IV) redox transition. DSA meshes generally have larger working areas for oxygen evolution than DSA plates and lead anodes.

The development of activated titanium anodes for oxygen evolution that are based on DSA (DSAs are widely used in chloride-alkaline electrolysis) can optimize the electrochemical behavior in the hydrometallurgical processes for the production of pure metals (Cu, Zn, Co, Cd, etc.). Such an anodic material would allow operation with a small and constant gap between the electrodes and without contamination of the electrolyte by metal dissolved from the anodes. This can result in decreased electrical energy consumption and increased cell productivity [7].

Iridium oxide alone or in combination with other less expensive oxides has attracted attention as a possible anode coating for oxygen evolution [8]. Thus, attempts have been made to test an IrO_2-coated anode in a laboratory copper winning cell [9]. To make iridium cost

Foundation item: Project (RDCPJ 428402) supported by the Natural Sciences and Engineering Research Council of Canada
Corresponding author: Wei ZHANG; Tel: +1-418-6562131, ext. 8657; Fax: +1-418-6565343; E-mail: Wei.zhang.1@ulaval.cA
DOI: 10.1016/S1003-6326(16)64121-3

effective, it is heavily doped or mixed with oxides of non-noble metals, such as Ti, Zr, Ta, Sn, Mn, Co [10−13]. Already, there exist a number of examples of composite materials used for oxygen-evolving anodes, such as Co_3O_4 particles [14], mechanically treated SnO_2 [15], $Ir_{0.15}O_{0.85}O_2$ [16].

MnO_2 was used to prepare OCA on a conductive polymeric substrate of polypropylene, rubber, graphite fiber and carbon black [17]. A wide variety of techniques for applying the pressed oxide coatings were evaluated before a suitable method was chosen. Hot pressed MnO_2 coatings into a carbon−polypropylene composite substrate showed better results [1]. MnO_2 was considered in this study to fabricate the pressed oxide powder coatings electrode.

The aim of this work is to investigate a suitable OCA which could decrease the overpotential of oxygen evolution reaction in zinc electrowinning practice. The anode should have a good stability with low corrosion rate during the polarization and potential decay. Also, the factor that influences the fabrication method such as the number of coating layer on the substrate of Ti/(30%IrO_2−70%Ta_2O_5) samples was examined. Then, the performance of one mesh and one plate anodes composed of Ti/(30%IrO_2−70%Ta_2O_5) and a second mesh anode with the composition of Ti/MnO_2 was studied in a zinc electrolyte at a current density of 50 mA/cm^2 and 38 °C, close to industrially utilized conditions. Electrochemical techniques, such as open-circuit potential (OCP) measurements, galvanostatic measurements, cyclic voltammetry and potentiodynamic measurements were employed to characterize the electrochemical behavior of the mesh and plate OCAs. In addition, a conventional Pb−0.7%Ag anode was considered for galvanostatic polarizability studies.

2 Experimental

2.1 Materials and sample preparation

A conventional thermodecomposition technique was used to prepare the oxide coatings [18]. The substrate for all the anodes was degreased, etched in 3.0 mol/L HCl solution, and then rinsed with deionized water. The 1.4 mm × 2 mm × 0.4 mm Ti/(IrO_2−Ta_2O_5) mesh (experimental area of 2.13 cm^2) and the 1 mm × 1 mm × 0.4 mm Ti/(IrO_2−Ta_2O_5) plate (experimental area of 1 cm^2) anodes were mainly fabricated from Ti/(30%IrO_2−70%Ta_2O_5). The precursors were prepared by mixing the necessary amounts of $H_2IrCl_6{\cdot}6H_2O_2$ and $TaCl_5$ in alcohol and isopropanol (volume ratio of 3:5) solutions. Then, the substrates were painted with coating solution using brushes. The plate substrate was brushed three layers of coating, while mesh substrate was brushed five layers of coating. The 1.4 mm × 2.3 mm × 0.4 mm (experimental area of 2.56 cm^2)Ti/MnO_2 mesh consists of a Ti substrate coated by a MnO_2 layer, employing power spray on the mesh Ti substrate.

The Ti/(IrO_2−Ta_2O_5) mesh, Ti/(IrO_2−Ta_2O_5) plate, and Ti/MnO_2 mesh anodes were connected with a copper wire isolated with plastic and cast in glue, leaving 2, 0.85 and 2.5 cm^2 of exposed surface areas, respectively. The fresh, as-received surfaces of the mesh and plate anodes were employed to perform the cyclic voltammetry studies. The composition of the Pb−0.7%Ag plate anode examined is given in Table 1. At least 45 elements were analysed by fluorescence X and only the elements with the mass fraction higher than 0.05% were given. The Ag, Ti and Fe contents were analysed quantitatively by atomic absorption technique. It was cut into small pieces of 1 cm × 1 cm × 1 cm, connected with a copper wire isolated with plastic and cast in acrylic resin, leaving exposed surface area of 1 cm^2. The surface was polished, ground with 600 soft grit SiC paper, and rinsed with ethanol to avoid the inclusion of SiC particles into the electrodes.

Table 1 Chemical composition of Pb−0.7%Ag anode (mass fraction, %)

Ag	Fe	Ca	Al	Mn
0.684	0.015	<0.001	<0.05	<0.05
S	Si	Ti	Zr	Pb
<0.05	0.23	0.19	0.2	Bal.

The composition of the electrolyte is similar to that currently used in industrial practice: 60 g/L Zn^{2+}, 180 g/L H_2SO_4, 8 g/L Mn^{2+}, 250 mg/L Cl^-, 3 mg/L glue. Zinc sulfate ($ZnSO_4{\cdot}7H_2O$) and manganese sulfate ($MnSO_4{\cdot}H_2O$) from Sigma-Aldrich Fine Chemicals and sodium chloride and sulfuric acid from Merck KGaA were used to prepare the supporting electrolyte with doubly distilled water. Gelatin (glue) was a product of BDH Inc. The chemicals meet analytical chemical standard (ACS) specifications (except for the gelatin) and were used as-received without further treatment. All the concentrations of H_2SO_4 and Zn^{2+} stated were the initial concentrations.

The cathodes were prepared from Al alloy (for current-efficiency measurements) or Pt (for corrosion-rate measurements). The reference electrode was a mercurous sulfate electrode (MSE): Hg, Hg_2SO_4/K_2SO_{4sat}, and a saturated K_2SO_4 salt bridge, which is used close to the anode (0.636 V (vs SHE)). Ag, $AgCl/KCl_{sat}$ (0.202 V (vs SHE)) was employed as the reference electrode in the electrochemical-noise measurements (ENM). All the potentials are with respect to the standard hydrogen electrode (SHE) reference.

2.2 Experimental setup

The electrolyte (1000 mL) was introduced into a double-walled beaker cell and heated by a flow of thermostated water (38±0.2) °C. The working electrode and the counter electrode were mounted in a suitable Teflon holder, and the distance between them was fixed at 2 cm. The experimental device was an EG&G PARSTAT 2263 potentiostat/galvanostat controlled by an IBM computer.

The standard ASTM G61−86 [19] was used to perform the cyclic potentiodynamic polarization. The cyclic potentiodynamic curves were traced at a scan rate of 20 mV/s without solution agitation. For the Pb−Ag alloy electrodes, the range was from −300 to 1800 mV versus the OCP. The measurements of the potentials of the mesh and plate anodes were performed by galvanostatic polarization at a current density of 50 mA/cm^2 and 38 °C. The standard ASTM G5−94 [20] was employed to perform the potentiodynamic test, and the potentiodynamic curves were traced at a scan rate of 0.166 mV/s and a scan potential range of 50 mV with a cathodic polarization of −25 mV versus the corrosion potential.

ENM were performed using a setup in the electrochemical noise (EN) mode of a zero-resistance ammeter (ZRA) without agitation. Two identical specimens were used as the working electrodes and a saturated silver chloride electrode (Ag, AgCl/KCl$_{sat}$ (0.202 V vs SHE)) was used as the reference electrode. The electrochemical current noise was measured as the galvanic coupling current between the two identical working electrodes (WE) maintained at the same potential. A potentiostat GAMRY model PC4/750 linked to a personal computer was used to log the potential, and current values sampled at a scan rate of 10 Hz for 102.4 s, giving a total of 1024 readings. The EN experiments and the data treatment were calculated using the GAMRY ESA400 software [21]. The noise data were collected for a 16 h immersion of the working electrodes by ENM in the solution, following a 24 h of polarization at a current density of 50 mA/cm^2. The noise data were also transformed into the frequency domain using a fast Fourier transform (FFT) algorithm and presented as the power spectral density (PSD), calculated in the frequency domain from 0.05 to 5 Hz.

The electrolyte was magnetically stirred at 412 r/min by a stirrer (4 cm in length and 1 cm in diameter) during all of the electrochemical measurements except for the CV and ENM tests.

Duplicate measurements were performed for all of the experiments, and triplicates were considered in certain cases, as discussed below. For example, the reproducibility of the potential, corrosion current density, and ENM values were ±3%, ±4% and ~5%, respectively.

2.3 Consecutive series of electrochemical testing

The following series of experiments were considered: a 2 h of open-circuit potential, linear polarization; a 24 h of polarization, linear polarization; a potential decay period of 16 h during which the electrochemical noise measurement mode of the zero-resistance ammeters (ZRA) was used, followed by linear polarization. An additional potential decay period of 6 h and a linear polarization measurement were performed to determine the corrosion potential (φ_{corr}) and the corrosion current density (J_{corr}) each time.

3 Results and discussion

3.1 Open-circuit potential measurements

In the 2 h of OCP tests, a two-electrode arrangement, involving the working reference (anode specimen) and the reference electrode, was used. The potential resulting from the electrochemical reactions at the anode/solution interface was then recorded by the potentiostat for a period of 2 h for the three specimens (Fig. 1).

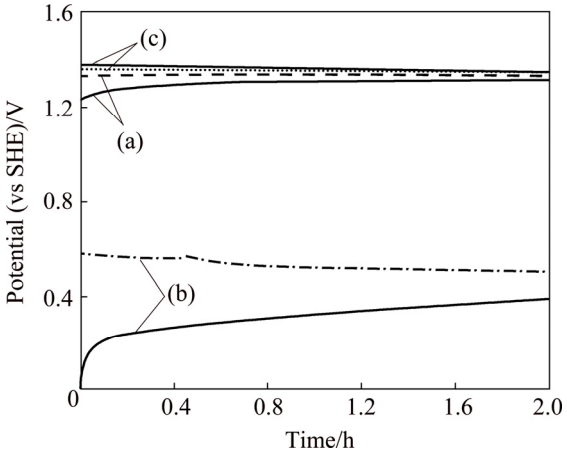

Fig. 1 Open-circuit potential (OCP) of fresh, as-received surfaces for Ti/(IrO_2−Ta_2O_5) mesh (a), Ti/MnO_2 mesh (b) and Ti/(IrO_2−Ta_2O_5) plate (c) anodes in zinc sulfate solution magnetically stirred at pH value of 0.2 and 38°C, shown in duplicates

Figure 1 shows that the Ti/(IrO_2−Ta_2O_5) mesh electrodes remain relatively stationary. One of the two curves for Ti/MnO_2 mesh decreases slowly from 0.55 to 0.48 V (vs SHE), the other increases sharply from 0 to 0.16 V at the beginning 15 min, then increases slowly until the end of 2 h experiment. The potential of the Ti/(IrO_2−Ta_2O_5) plate electrode remains almost stationary for 2 h. After 2 h of OCP test, the Ti/(IrO_2−Ta_2O_5) plate electrode obtains the highest potential (1.363±0.013) V among the three anodes, followed by the Ti/(IrO_2−Ta_2O_5) mesh (1.312±0.019) V, and finally by the Ti/MnO_2 mesh (0.561±0.160) V (Fig. 1).

It can be seen that the results of the duplicate measurements of the corrosion potential for the Ti/(IrO_2−Ta_2O_5) plate and mesh specimens are satisfactory (±1%). In contrast, the Ti/MnO_2 mesh electrode specimen gives a large deviation in the potential after 2 h of OCP test. However, the difference in the OCP values for the Ti/MnO_2 samples is very small (less than 8 mV) after 5 h (not shown in Fig. 1).

3.2 Corrosion rate from linear polarization

After 2 h of OCP test, a linear polarization of the three anodes was performed, and the results are shown in Table 2.

Table 2 Corrosion potentials and corrosion current densities determination after 2 h of OCP test by linear polarization of three specimens in stirred zinc sulfate solution (pH value of 0.2) at 38 °C

Anode	Corrosion potential (vs SHE)/V	Corrosion current density /(μA·cm^{-2})
Ti/(IrO_2−Ta_2O_5) mesh	1.316±0.011	3.37±1.84
Ti/MnO_2 mesh	0.518±0.188	223.5±92
Ti/(IrO_2−Ta_2O_5) plate	1.358±0.023	10.51±1.22

After 2 h of polarization, the corrosion potentials, as deduced from the linear polarization studies, confirmed the results obtained from the open-circuit potential measurements in Fig. 1. The corrosion potential values of the mesh electrode (Ti/MnO_2) were not reproducible. However, the average value of potential (0.518 V) of the Ti/MnO_2 mesh specimen is much lower than the reproducible values of the Ti/(IrO_2−Ta_2O_5) plate (1.358 V) and mesh (1.316 V) anodes (Table 2).

The corrosion current density of the Ti/(IrO_2−Ta_2O_5) mesh electrode is the lowest ((3.37±1.84) μA/cm^2) among the three electrodes. The corrosion current density of the Ti/(IrO_2−Ta_2O_5) plate is higher than that of the Ti/(IrO_2−Ta_2O_5) mesh electrode. However, it is significantly lower than that of the Ti/MnO_2 mesh, which is extremely high ((223.5±92) μA/cm^2) compared with the values of other two electrodes. The high current density of the MnO_2 electrode (Table 2) could be expected because of the depolarization of the cathodic hydrogen reaction and the instability of the electrode.

3.3 Galvanostatic measurements and potential decay by electrochemical-noise measurements

In galvanostatic measurements or chronopotentiometry, a constant current density (50 mA/cm^2) was applied between the auxiliary and working electrodes. The working electrode potential was recorded as a function of time with respect to the reference electrode. Figure 2 shows the performance of the three OCAs and the Pb−Ag anode under oxygen evolution conditions at a current density of 50 mA/cm^2. It can be observed that after 24 h of polarization, the Ti/MnO_2 mesh anode has the highest potential ((1.799±0.023) V) among the three anodes, followed by the Ti/(IrO_2−Ta_2O_5) plate ((1.775±0.013) V) and finally the Ti/(IrO_2−Ta_2O_5) mesh ((1.705±0.016) V). However, the conventional Pb−0.7%Ag anode (1.950 V) has a much higher potential than the three OCAs. Compared with that of the Pb−0.7%Ag (1.950 V) anode, the potentials for the Ti/MnO_2 mesh, Ti/(IrO_2−Ta_2O_5) plate and Ti/(IrO_2−Ta_2O_5) mesh anodes are 7.8%, 9% and 12.6% lower, respectively, at the end of 24 h of polarization. The Ti/(IrO_2−Ta_2O_5) mesh anode specimen has the most active or the lowest potential, possibly corresponding to the best performance.

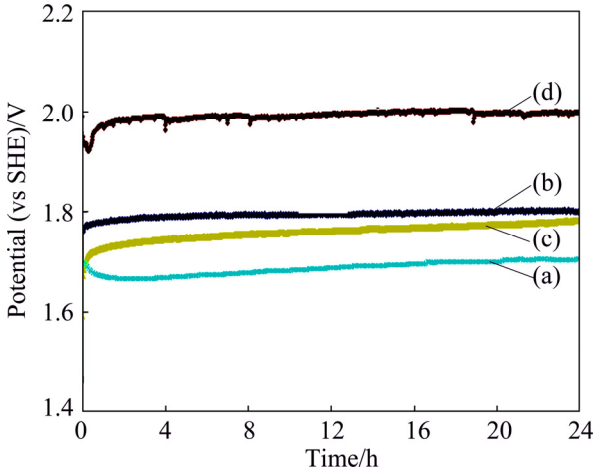

Fig. 2 Potentials of Ti/(IrO_2−Ta_2O_5) mesh (a), Ti/MnO_2 mesh (b), Ti/(IrO_2−Ta_2O_5) plate (c) and Pb−0.7%Ag (d) anodes at current density of 50 mA/cm^2 in acidic zinc sulfate electrolyte magnetically stirred at 38 °C

As shown in Fig. 2, the curve of the Pb−Ag anode has some remarkable fluctuations, however, those of the Ti/(IrO_2−Ta_2O_5) mesh, Ti/MnO_2 mesh, and Ti/(IrO_2−Ta_2O_5) plate anodes have generally less and/or small fluctuations. The fluctuations of the anode potential are probably due to the repeated formation and breakdown of the anode film. For example, in the case of non-conductive Ti/MnO_2 mesh, MnO_2 forms on the surface of the polished anode, and gradually covers the surface of the anode, then, the current density of the small uncovered conductive parts of the anode increases rapidly, and this causes the anode film breakdown into the electrolyte. The dense non-conductive and well adherent MnO_2 film, that increases the thickness and density of oxide layer, can form according to the following equations [22]:

$$MnSO_4+2H_2O-2e=MnO_2+H_2SO_4+2H^+ \quad (1)$$

$$MnSO_4+4H_2O-5e=MnO_4^-+H_2SO_4+6H^+ \quad (2)$$

$$3MnSO_4+2HMnO_4+2H_2O=5MnO_2+3H_2SO_4 \quad (3)$$

3.4 Cathodic current efficiencies

The cathodic current efficiencies after 24 h of galvanostatic polarization at 50 mA/cm^2 were calculated, considering the practical mass of the deposit and the theoretical, quantitative Faraday law (current quantity and equivalent mass). The cathodic current efficiencies measured for the two mesh anodes and the plate anode in an acidic zinc sulfate electrolyte at 38 °C are given in Table 3.

Table 3 Cathodic current efficiencies after 24 h of galvanostatic polarization at 50 mA/cm^2 of three OCAs and Pb−0.7%Ag anode in zinc electrolyte magnetically stirred at 38 °C

Anode	Current efficiency/%			
	1st run	2nd run	3rd run	Average value
Ti/(IrO_2−Ta_2O_5) mesh	92.3	92.7	92.4	92.5
Ti/MnO_2 mesh	94.5	94.6	94.6	94.6
Ti/(IrO_2−Ta_2O_5) plate	93.1	92.7	92.6	92.8
Pb−0.7%Ag	92.2	92.4	92.3	92.3

Table 3 shows that the Ti/MnO_2 mesh anode has the highest current efficiency (94.6%) among the three OCA specimens, followed by the Ti/(IrO_2−Ta_2O_5) plate and the Ti/(IrO_2−Ta_2O_5) mesh with close values (~92.7%). The Ti/MnO_2 mesh anode has the highest current efficiency because the MnO_2 coating can influence the chemical and/or electrochemical reactions.

3.5 Linear polarization

After 24 h of galvanostatic polarization, the linear polarization of the two mesh anodes and the Ti/(IrO_2−Ta_2O_5) plate was tested. The results are shown in Table 4.

Table 4 shows that the Ti/MnO_2 mesh anode has the highest potential among the three specimens, followed by the Ti/(IrO_2−Ta_2O_5) plate anode and the Ti/(IrO_2−Ta_2O_5) mesh anode. Additionally, the Ti/MnO_2 mesh has the highest corrosion current density among the three specimens, followed by the Ti/(IrO_2−Ta_2O_5) plate and Ti/(IrO_2−Ta_2O_5) mesh anodes. Although the Ti/MnO_2 mesh anode has the highest current efficiency among the three anodes, it also shows the highest corrosion current density. It is possible that the Ti/MnO_2 mesh anode and/or its corrosion products are easy to dissolve in an acidic sulfate solution.

Table 4 Corrosion potentials and corrosion current densities of three OCA specimens after 24 h of galvanostatic polarization in zinc electrolyte magnetically stirred at 38 °C

Anode	Corrosion potential (vs SHE)/V	Corrosion current density/(μA·cm^{-2})
Ti/(IrO_2−Ta_2O_5) mesh	1.443±0.019	134±13
Ti/MnO_2 mesh	1.649±0.011	625.6±185
Ti/(IrO_2−Ta_2O_5) plate	1.493±0.014	228±8

3.6 Potential decay after polarization

3.6.1 Zero-resistance ammeters (ZRA) during 16 h discharge after 24 h of electrolysis

After 24 h of polarization at a current density of 50 mA/cm^2 and 38 °C, a 16 h of decay of the two mesh and one plate anodes in an acidic zinc sulfate electrolyte were performed by an electrochemical-noise measurement. The results are shown in Fig. 3.

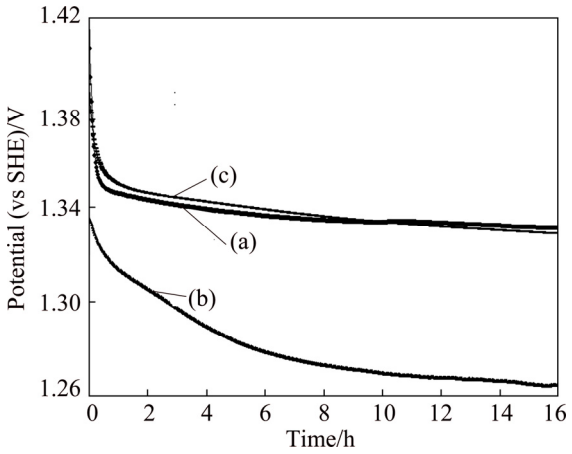

Fig. 3 Potential decay transient curves of Ti/(IrO_2−Ta_2O_5) mesh (a), Ti/MnO_2 mesh (b) and Ti/(IrO_2−Ta_2O_5) plate (c) anodes representing trend during immersion time of 16 h following 24 h of polarization at 50 mA/cm^2 in zinc electrolyte solution at 38°C without agitation

Figure 3 shows that the Ti/MnO_2 mesh anode has a more rapid decay than other two anodes, the Ti/(IrO_2−Ta_2O_5) mesh and Ti/(IrO_2−Ta_2O_5) plate anodes, which have similar decay rates. During the 16 h of decay, the potential of the Ti/MnO_2 mesh anode drops almost 0.07 V. It is possible that reduction reactions occur during the 16 h of decay in the zinc electrolyte for the Ti/MnO_2 mesh anode as follows [22]:

$$MnOOH+3H^++e=Mn^{2+}+2H_2O,\ \varphi_0=1.183\ V \quad (4)$$

$$MnO_2(s)+4H+2e=Mn^{2+}+2H_2O,\ \varphi_0=1.228\ V \quad (5)$$

$$MnO_4^-+8H^++5e=Mn^{2+}+4H_2O,\ \varphi_0=1.512\ V \quad (6)$$

It can be deduced from the following MnOOH, MnO_2 and MnO_4^- reduction reactions that MnO_2 can be reduced to Mn^{2+} and dissolved in the acidic sulphate zinc electrolyte solution.

For the Ti/(IrO_2−Ta_2O_5) mesh and plate anodes, one reduction occurs on the surfaces of these two anodes as follows [23]:

$$IrO_2(OH)+2H^++2e\longrightarrow Ir(OH)_3,\ \varphi_0=0.926\ V \quad (7)$$

3.6.2 Admittance ($1/R_n$) during decay period of 16 h

The most interesting parameter of the statistical analysis in the time domain is the noise resistance (R_n), defined as the ratio of the standard deviation of the potential noise to that of the current noise, which is associated with the polarization resistance (R_p). The inverse R_n is the admittance with the unit of Siemens (S), which is proportional to the corrosion rate [24,25]. After 24 h of polarization in the zinc electrolyte, an evolution of the admittance ($1/R_n$) during the 16 h of decay was performed for the three specimens. Continuously, in situ measurements were summarized every 1 h into one point by statistics (Fig. 4). This shows that the Ti/MnO_2 mesh anode has the highest corrosion rate (79.2 mS/cm^2) among the three specimens, followed by the Ti/(IrO_2−Ta_2O_5) plate (45.6 mS/cm^2) and the Ti/(IrO_2−Ta_2O_5) mesh (24.1 mS/cm^2) after the 16 h of decay following the 24 h of polarization at 50 mA/cm^2. Therefore, the Ti/(IrO_2−Ta_2O_5) mesh anode performed better than the Ti/MnO_2 mesh and Ti/(IrO_2−Ta_2O_5) plate anodes during the current interruption.

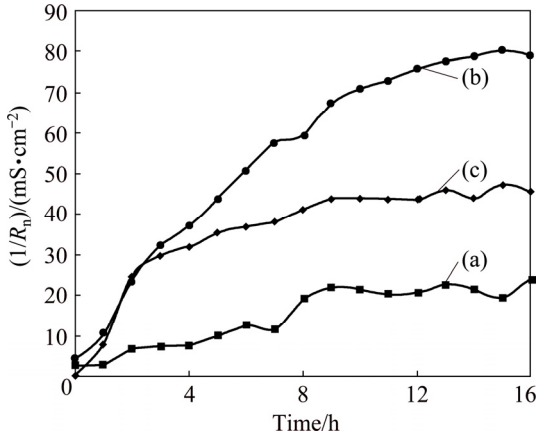

Fig. 4 Evolution of admittance ($1/R_n$) of Ti/(IrO_2−Ta_2O_5) mesh (a), Ti/MnO_2 mesh (b), and Ti/(IrO_2−Ta_2O_5) plate (c) anodes recorded during immersion period of 16 h in zinc electrolyte without agitation

3.7 Linear polarization

After the 16 h of decay following the 24 h of galvanostatic polarization, a linear polarization of the three OCAs was performed, and the results are shown in Table 5.

Table 5 Corrosion potentials and corrosion current densities of specimens in zinc electrolyte magnetically stirred at 38 °C after 16 h of decay following 24 h of galvanostatic polarization

Anode	Corrosion potential (vs SHE)/V	Corrosion current density/(μA·cm^{-2})
Ti/(IrO_2−Ta_2O_5) mesh	1.300±0.008	7.9±1.6
Ti/MnO_2 mesh	1.156±0.024	429.2±99.6
Ti/(IrO_2−Ta_2O_5) plate	1.367±0.016	21.5±5.7

The Ti/MnO_2 mesh anode obtains the lowest potential and the highest corrosion rate (Table 5). The corrosion rate of the Ti/(IrO_2−Ta_2O_5) mesh (7.91 mS/cm^2) is very low, showing an excellent corrosion resistance in the zinc electrolyte. It is found that the difference between the corrosion rate of the Ti/(IrO_2−Ta_2O_5) mesh and those of other two anodes in Table 5 is much larger than the difference between the admittance of the Ti/(IrO_2−Ta_2O_5) mesh (24.1 mS/cm^2) and those of other two anodes in Fig. 4. This is because the admittance was obtained during the decay period by electrochemical noise without agitation, whereas the corrosion rate was obtained during the polarization after the decay, and the solution was magnetically stirred at 412 r/min. This resulted in a variation in the oxygen concentration at the interface of the specimens in the zinc electrolyte.

3.8 Last 6 h of potential decay

Figure 5 shows the potential decay transient curves of the mesh and plate anodes, representing the trend during an additional immersion time of 6 h, following the 16 h of decay after the 24 h of polarization (50 mA/cm^2) in a zinc electrolyte solution at 38 °C.

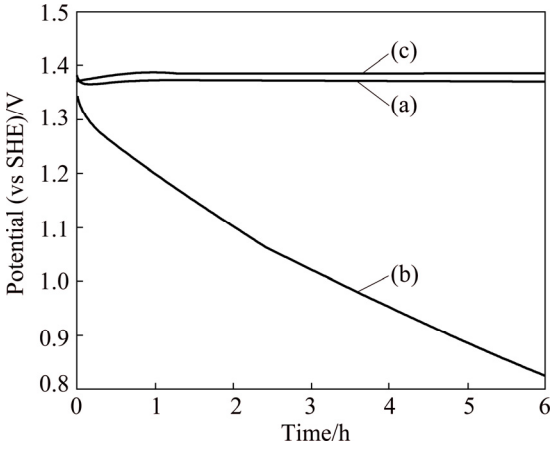

Fig. 5 Potential decay transient curves of Ti/(IrO_2−Ta_2O_5) mesh (a), Ti/MnO_2 mesh (b), Ti/(IrO_2−Ta_2O_5) plate (c) anodes, representing trend during additional immersion time of 6 h, following 16 h of decay after 24 h of polarization at 50 mA/cm^2 in zinc electrolyte solution magnetically stirred at 38 °C

The Ti/MnO_2 mesh anode has a much quicker decay than the Ti/(IrO_2−Ta_2O_5) plate and Ti/(IrO_2−Ta_2O_5) mesh anodes. The potential decay of the Ti/MnO_2 mesh anode decreases from 1.358 to 0.841 V during the 6 h of decay. However, the values for other two anodes only fall about 50 mV. This means that the coating of the Ti/MnO_2 mesh undergoes reduction of its oxidized state during this decay, and this is reversible to its starting "OCP" before galvanostatic polarization; however, the other two anodes keep their initial high OCP values.

3.9 Final linear polarization at open-circuit potential

After a 6 h of decay following the 16 h of decay and 24 h of galvanostatic polarization, linear polarization of the three anodes was performed, and the results are shown in Table 6.

Table 6 Corrosion potentials and corrosion current densities of specimens in stirred zinc electrolyte after final 6 h of decay following 24 h of galvanostatic polarization and 16 h of decay period

Anode	Corrosion potential (vs SHE)/V	Corrosion current density/(μA·cm^{-2})
Ti/(IrO_2−Ta_2O_5) mesh	1.378±0.011	5.13±2.1
Ti/MnO_2 mesh	0.849±0.018	458.4±112
Ti/(IrO_2−Ta_2O_5) plate	1.384±0.013	10.35±1.35

Table 6 shows that the Ti/(IrO_2−Ta_2O_5) mesh and plate anodes have approximately the same potential (~1.380 V), which is higher than that of the Ti/MnO_2 mesh anode (0.849 V). The corrosion current density of the Ti/(IrO_2−Ta_2O_5) mesh anode is the lowest among the three specimens, followed by the Ti/(IrO_2−Ta_2O_5) plate and Ti/MnO_2 mesh anodes. The corrosion current density of the Ti/(IrO_2−Ta_2O_5) mesh is only 5.13 μA/cm^2, and it is similar to that of Pb−0.7%Ag after the 6 h of decay following the 16 h of decay and 24 h of galvanostatic polarization [26]. This means that the coating of the Ti/(IrO_2−Ta_2O_5) mesh is resistant in the sulfate acid solution during the zinc electrowinning. It can also be mentioned that the Ti/(IrO_2−Ta_2O_5) mesh has a lower overpotential and corrosion rate than the Pb−0.7%Ag anode during the zinc electrowinning. However, it can also be observed that the reproducibility of the corrosion rates of the Ti/MnO_2 mesh anode is not good because the anode is not stable in an acidic sulfate medium.

It should be noted that the Ti/(IrO_2−Ta_2O_5) mesh anode has the same composition as the Ti/(IrO_2−Ta_2O_5) plate anode. However, the corrosion rate of the Ti/(IrO_2−Ta_2O_5) mesh anode is lower than that of the Ti/(IrO_2−Ta_2O_5) plate anode. This is possibly because the Ti/(IrO_2−Ta_2O_5) mesh anode was perfectly manufactured with 5 coating layers on the Ti substrate. In spite of higher real surface of the exposed mesh anode, the plate shows much higher corrosion rate, very possibly because of adhesion of surface conditioning and possibly three layers are not enough or weakly integrated on the anode. These factors allow the Ti/(IrO_2−Ta_2O_5) mesh anode to have much better electrochemical behavior in the zinc electrolyte than the Ti/(IrO_2−Ta_2O_5) plate anode.

3.10 Voltammetric characteristics

In situ cyclic voltammetry measurements without agitation can probe sensitively the surface behavior of an electrode. Figure 6 shows typical CV curves for each of the three fresh surfaces of OCAs in a 180 g/L H_2SO_4 solution at 38 °C and a scan rate of 20 mV/s. The potential region ranges from −0.3 to 1.8 V (vs SHE) in Fig. 6(a). In Fig. 6(b), the potential range is from 1.0 to 1.9 V (vs SHE).

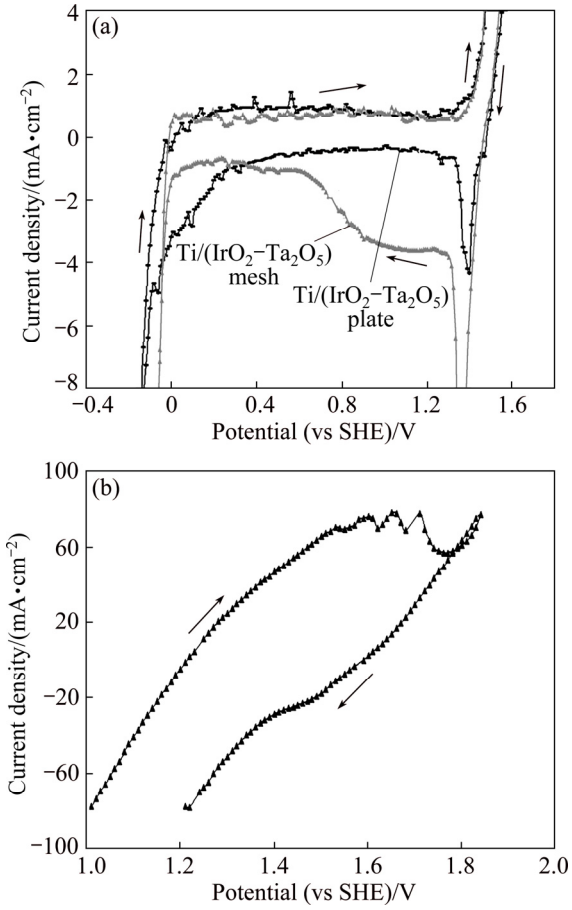

Fig. 6 Cyclic voltammetry of Ti/(IrO_2−Ta_2O_5) mesh anode and Ti/(IrO_2−Ta_2O_5) plate anode (a), and as-received Ti/MnO_2 mesh anode (b) at 20 mV/s and 38 °C in 180 g/L H_2SO_4 solution saturated with atmospheric oxygen without agitation

It can be seen from Fig. 6(a) that there are one oxidation reaction (oxygen evolution: $2H_2O \rightarrow O_2+4H^+ + 4e$) and one reduction reaction ($Ir(OH)_3 \rightarrow IrO_2(OH)+2H^+ +2e$ [23]) on the curves of Ti/(IrO_2−Ta_2O_5) mesh anode and Ti/(IrO_2−Ta_2O_5) plate anode. The starting potential of the oxygen evolution of the Ti/(IrO_2−Ta_2O_5) mesh anode in 180 g/L H_2SO_4 solution is at 1.31 V, then, the scan potential goes up to one point (around 1.45 V, not shown) and arrives to 1.52 V. That is almost identical to that of the Ti/(IrO_2−Ta_2O_5) plate anode. Additionally, it can be observed that the scan current area which is between the oxidation and reduction curves [2] of Ti/(IrO_2−Ta_2O_5) mesh (1.8 mA·V) is larger than that of Ti/(IrO_2−Ta_2O_5) plate (1.3 mA·V). This means that the Ti/(IrO_2−Ta_2O_5) mesh anode has better electrocatalytic properties than Ti/(IrO_2−Ta_2O_5) plate anode [3,27]. Figure 6(b) shows that there are four positive peaks in

the curve of Ti/MnO_2 mesh anode. Also, the negative current density can be observed. It is very possible that one oxidation reaction (oxygen evolution) and three reduction reactions of Mn ion: $MnOOH+3H^++e=Mn^{2+}+2H_2O$, $MnO_2(s)+4H^++2e=Mn^{2+}+2H_2O$, and $MnO_4^-+8H^++5e=Mn^{2+}+4H_2O$ [22] happen, as shown in Fig. 6 (b). Since the positive current density of Ti/MnO_2 mesh anode is much higher (around 90 mA/cm^2) as compared with that of Ti/(IrO_2−Ta_2O_5) mesh and plate anodes, this means that the oxide reaction of Mn^{2+} is very strong.

3.11 SEM morphologies of three OCAs and Pb−0.7%Ag anode

The SEM images of Ti/(IrO_2−Ta_2O_5) mesh, Ti/(IrO_2−Ta_2O_5) plate, Ti/MnO_2 mesh and Pb−0.7%Ag anodes after 24 h of polarization in a zinc sulfate solution followed by 16 h of decay at pH value of 0.2 and 38 °C are shown in Fig. 7. It is found that there are deep cracks on the coating of Ti/(IrO_2−Ta_2O_5) mesh anode (Fig. 7(a)), whereas the surface coating is much smoother for the plate anode (Fig. 7(c)).

Figure 7(b) shows many cracks on the Ti/MnO_2 mesh coating, and the MnO_2 mesh coating is heterogeneous with a mud-cracked morphology. The crystals of MnO_2 coating are loose, and almost every crystal of MnO_2 coating contains a hole. It means that the crystal is corroded easily in the sulfuric acid solution. For the Ti/(IrO_2−Ta_2O_5) plate anode, the coating surface is smoother than that of the MnO_2 coating. However, there are shallow cracks on the coating surface (Fig. 7(c)). For the Pb−0.7%Ag anode, it is found that there are long size crystals (6−8 μm) in the film formed on the surface (Fig. 7(d)) while the three OCAs have the square and short crystals.

Figure 8 gives the element analysis results of the spots of the surfaces of the three anodes in Figs. 7(a, b and c) using energy dispersive X-ray analysis (EDX) technique. It can be seen that the Ti/(IrO_2−Ta_2O_5) mesh and plate anodes are richer in O, Ta and Ir elements (Figs. 8(a) and (c)), indicating that IrO_2 and Ta_2O_5 exist on the surface of the two catalytic anodes. The origin of Ti element should come from the substrate of the anode. Figure 8(b) shows that the anode is rich in Mn and O elements, since MnO_2 exists on the surface after polarization followed by 16 h of potential decay.

4 Conclusions

1) After 24 h of galvanostatic polarization at 50 mA/cm^2, the Ti/MnO_2 mesh anode exhibits the highest current efficiency (94.6%), followed by the Ti/(IrO_2−Ta_2O_5) plate (92.8%) and the Ti/(IrO_2−Ta_2O_5) mesh (92.5%), as compared with 92.3% of the conventional Pb−Ag anode.

2) After 24 h of polarization, the Ti/(IrO_2−Ta_2O_5) mesh anode has the lowest potential (1.705 V) among the

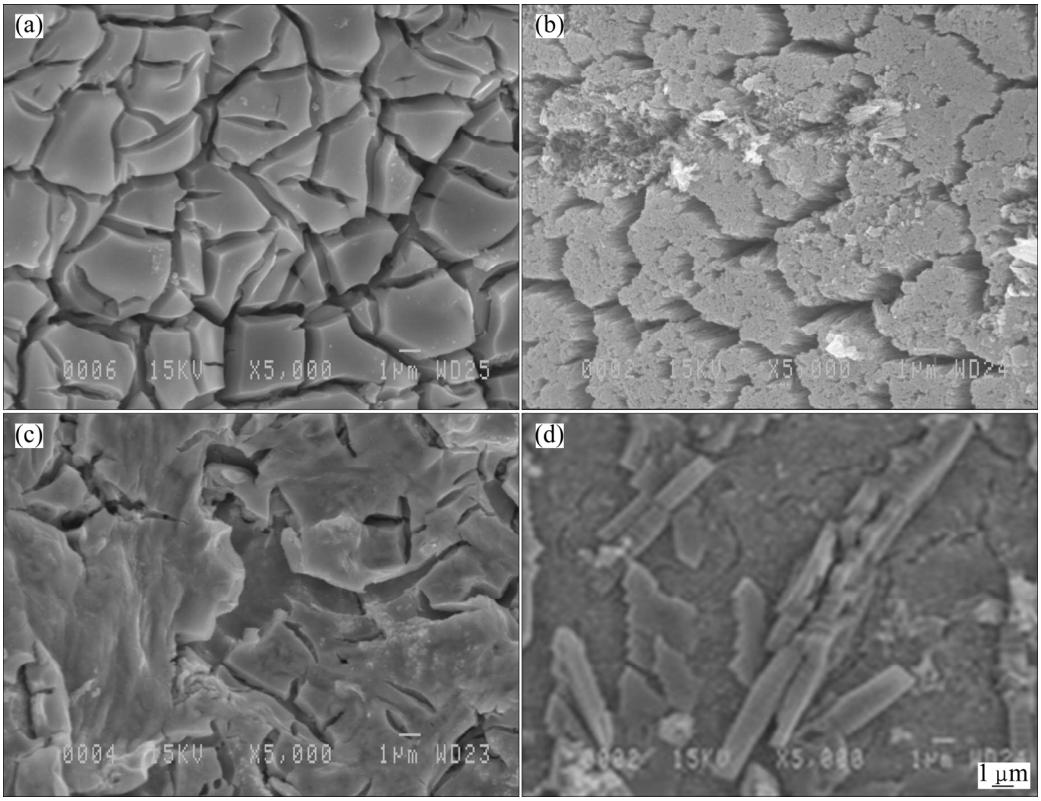

Fig. 7 SEM images of Ti/(IrO_2−Ta_2O_5) mesh anode (a), Ti/MnO_2 mesh anode (b), Ti/(IrO_2−Ta_2O_5) plate anode (c) and Pb−0.7%Ag anode (d)

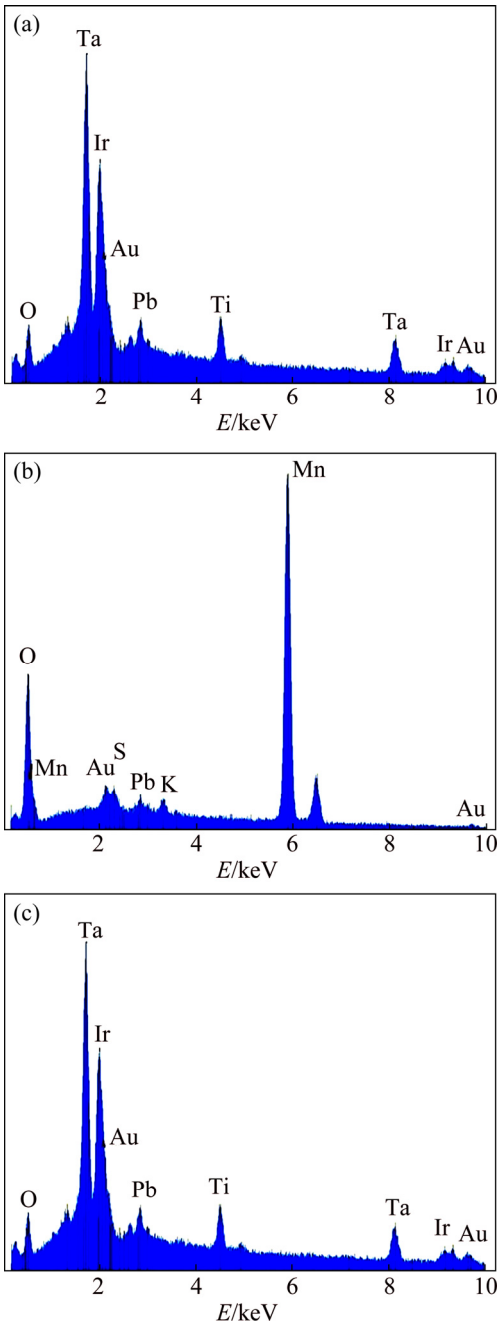

Fig. 8 EDX analysis of surfaces of Ti/(IrO_2−Ta_2O_5) mesh anode (a), Ti/MnO_2 mesh anode (b) and Ti/(IrO_2−Ta_2O_5) plate anode (c)

three OCA specimens, followed by the Ti/(IrO_2−Ta_2O_5) plate anode (1.775 V) and the Ti/MnO_2 mesh anode (1.799 V), whereas the potential of the Pb−0.7%Ag anode is 1.950 V.

3) At the end of 2 h of open-circuit potential (OCP), the as-received Ti/(IrO_2−Ta_2O_5) plate electrode exhibits the highest positive potential ((1.363±0.013) V) among the three anodes, followed by the Ti/(IrO_2−Ta_2O_5) mesh ((1.312±0.019) V) and finally the Ti/MnO_2 mesh ((0.561±0.160) V).

4) The electrochemical noise measurements show that after 24 h of polarization and 16 h of decay, the Ti/(IrO_2−Ta_2O_5) mesh anode has the lowest corrosion rate (24.1 mS/cm^2), followed by the Ti/(IrO_2−Ta_2O_5) plate (45.6 mS/cm^2) and Ti/MnO_2 mesh (79.2 mS/cm^2) anodes. The same tendency is obtained from the linear polarization measurements for the three anodes.

5) The cyclic voltammetry curves show that there are one oxygen evolution reaction and the Ir^{3+}/Ir^{5+} ion reduction reactions for the two Ti/(IrO_2−Ta_2O_5) mesh and plate anodes. However, for the Ti/MnO_2 mesh anode, the peaks are corresponding to three manganese oxidation reactions and one oxygen evolution reaction.

Acknowledgments

The authors are grateful to Hydro-Quebec and Xstrata zinc and the Natural Sciences and Engineering Research Council of Canada (NSERC) for their financial support.

References

[1] BRUNGS A, HADDADI-ASL V, SKYLLAS-KAZACOS M. Preparation and evaluation of electrocatalytic oxide coatings on conductive carbon-polymer composite substrate for use as dimensionally stable anodes [J]. J Appl Electrochem, 1996, 26: 1117−1123.

[2] MSINDO Z S, SIBANDA V, POTGIETER J H. Electrochemical and physical characterisation of lead-based anodes in comparison to Ti−(70%) IrO_2 (30%) Ta_2O_5 dimensionally stable anodes for use in copper electrowinning [J]. J Appl Electrochem, 2010, 40: 691−699.

[3] COMNINELLIS C H, VERCESI G P. Characterization of DSA-type oxygen evolving electrodes: Choice of a coating [J]. J Appl Electrochem, 1991, 21: 335−345.

[4] MORIMITSU M, TAMURA H, MATSUNAGA M, OTOGAWA R. Polarization behaviour and lifetime of IrO_2−Ta_2O_5−SnO_2/Ti anodes in p-phenolsulfonic acid solutions for tin plating [J]. J Appl Electrochem, 2000, 30: 511−514.

[5] KOTZ R, STUCKI S. Stabilization of RuO_2 by IrO_2 for anodic oxygen evolution in acid media [J]. Electrochim Acta, 1986, 31: 1311−1316.

[6] XIAO S J, MOKKELBOST T, PAULSEN O, RATVIK A P, HAARBERG G M. SnO_2-based gas (hydrogen) anodes for aluminum electrolysis [J]. Transactions of Nonferrous Metals Society of China, 2014, 24(12): 3917−3921.

[7] PAVLOVIC M G, DEKANSKI A. On the use of platinized and activated titanium anodes in some electrodeposition processes [J]. J Solid State Electrochem, 1997, 1: 208−214.

[8] KULANDAISAMY K, PRABHAKAR J, REABHKAR P, CHOCKALINGAM S C, VISVANATHAN S, VENKATESWARAN K V, RAMACHANDRAN P, NANAKUMAR V. Perfromance of catalytically activated anodes in the electrowinning of metals [J]. J Appl Electrochem, 1997, 27: 579−583.

[9] FERRON C G. Investigation of precious metal coated anodes in copper electrowinning [D]. New York: Columbia University, 1998: 77−89.

[10] ROLEWICZ J, COMMINELLIS C H, PLATTNER E, HINDEN J. Characterization of DSA type electrodes for release of O_2. I. Ti/IrO_2−Ta_2O_5 electrode [J]. Electrochim Acta, 1988, 33(4): 573−580. (in French)

[11] BALKO N, NGUYEN P H. Iridium-tin mixed oxide anode coatings [J]. J Appl Electrochem, 1991, 21: 678−682.
[12] MRAZ R, KRYSA J. Long service life IrO_2/Ta_2O_5 electrodes for electroflotation [J]. J Appl Electrochem, 1994, 24: 1262−1266.
[13] KAMEGAYA Y, SASAKI K, OGURI M, ASAKI T, KOBAYASHI H, MITAMURA T. Improved durability of iridium oxide coated titanium anode with interlayers for oxygen evolution at high current densities [J]. Electrochim Acta, 1995, 40: 889−895.
[14] NIKOLOSKI A N, NICOL M J. Addition of cobalt to lead anodes used for oxygen evolution—A literature review [J]. Mineral Processing and Extractive Metallurgy Review, 2010, 31(1): 30−57.
[15] PALMAS S, POLCARO A M, FERRARAL F, RUIZ J R, PELOGU F, BONATTO-MINELLA C, MULAS G. Electrochemical performance of mechanically treated SnO_x powders for OER in acid solution [J]. J Appl Electrochem, 2008, 38: 907−913.
[16] VERTOVA A, BORGESE L, GAPPELLETTI G, LOCATTELLI C, MINGUZZI A, PEZZONI C, RONDININI S. New electrocatalytic materials based on mixed metal oxides: Electrochemical quartz crystal microbalance characterization [J]. J Appl Electrochem, 2008, 38: 973−978.
[17] SCHMACHTEL S, TOIMIMEN M, KONTTURI K, FORSEN O, BARKER M H. New oxygen evolution anodes for metal electrowinning: MnO_2 composite electrodes [J]. J Appl Electrochem, 2009, 39: 1835−1848.
[18] HU J M, WU J X, ME H M, SUN D B, ZHU Y R, YANG D J. Degradation characteristic of Ti/(IrO_2+Ta_2O_5) coating anodes in H_2SO_4 solution [J]. Transactions of Nonferrous Metals Society of China, 2000, 10(4): 511−515.
[19] ASTM G61−86. Standard test method for conducting cyclic potentiodynamic polarization measurements for localized corrosion susceptibility of iron-, nickel-, or cobalt-base alloys [S].
[20] ASTM G5−94. Standard reference test method for making potentiostatic and potentiodynamic anodic polarization measurements [S].
[21] LAFRONT A M, ZHANG W, JIN S, TREMBLAY R, DUBE D, GHALI E. Pitting corrosion of AZ91D and AJ62x magnesium alloys in alkaline chloride medium using electrochemical techniques [J]. Electrochim Acta, 2005, 51: 489−501.
[22] IVANOV I, STEFANOV Y, NONCHEVA Z, PETROVA M, DOBREV T, MIRKOVA L, VERMEERSCH R, DEMAEREL J P. Insoluble anodes used in hydrometallurgy part I: Corrosion resistance of lead and lead alloy anodes [J]. Hydrometallurgy, 2000, 57: 109−124.
[23] KOTZ R, NEFF H, STUCKI S. Anodic iridium oxide films [J]. J Electrochem Soc, 1984, 131: 72−77.
[24] REVIE R W. Uhlig's corrosion Handbook [M]. New York: John Wiley, 2011: 1167−1177.
[25] COTTIS R, TURGOOSE S. Electrochemical impedance and noise [M]. Houston: NACE International, 1999.
[26] ZHANG W, LAFRONT A M, GHALI E, HOULACHI G, MONTEITH G, CHAMPOUX G. Effect of silver content in Pb−Ag anodes on the performance of the anodes during zinc electrowinning [J]. Canadian Metallurgical Quarterly, 2009, 48: 326−337.
[27] YAN Z W, MENG H M. Effect of heat treatment of titanium substrates on the properties of IrO_2−Ta_2O_5 coated anodes [J]. Rare Metals, 2011, 30: 439−446.

网状和片状氧化涂层阳极在电解锌过程中的电化学行为

张 伟[1,2]，Michael ROBICHAUD[2], Edward GHALI[2], Georges HOULACHI[3]

1. 湖南工业大学 冶金工程学院，株洲 412007;
2. Department of Mining, Metallurgy and Material Engineering, Laval University, Ste-Foy, Quebec G1K 7P4, Canada;
3. Hydro-Quebec Research Center, Shawinigan, Quebec G9N 7N5, Canada

摘 要：研究两个网状和一个片状氧化涂层阳极在 38 °C 的电解锌溶液中的催化性能，并与通用的 Pd−0.7%Al 合金的电化学性能进行对比。采用电化学测试方法进行实验，如循环动电位法、恒电流法、动电位法、开路电位法和原位电化学噪音法。经过 2 h 的开路电位实验，线性极化结果表明：网状 Ti/(IrO_2−Ta_2O_5)电极显示出非常好的性能，其腐蚀电流密度在三个氧化涂层阳极中是最低的(3.37 μA/cm^2)。此外，在 50 mA/cm^2 和 38 °C 的条件下，经过 24 h 的恒电流极化试验，网状 Ti/MnO_2 阳极有最高的电位(1.799 V)，紧随其后的是片状 Ti/(IrO_2−Ta_2O_5)(1.775 V)和网状 Ti/(IrO_2−Ta_2O_5)阳极(1.705 V)。经过 24 h 的恒电流极化和 16 h 时的电位衰退实验后，线性极化方法验证了经过 2 h 的开路电位实验得出的结果，即网状 Ti/(IrO_2−Ta_2O_5)阳极有最低的腐蚀电流。网状 Ti/(IrO_2−Ta_2O_5)阳极在 24 h 极化后显示出更好的性能，并与通用的 Pb−0.7%Al 合金进行相比，过电位低~245 mV。

关键词：氧化涂层阳极；网状；片状；电化学测量；电化学性能

(Edited by Mu-lan QIN)